Brain Stimulation 15 (2022) 1418–1431

Contents lists available at ScienceDirect

Brain Stimulation

journal homepage: http://www.journals.elsevier.com/brain-stimulation

Maximizing brain networks engagement via individualized connectome-wide target search

Arianna Menardi [a, b], Davide Momi [c, j], Antonino Vallesi [b], Albert-László Barabási [d, e, f], Emma K. Towlson [g, h, i, k, 1], Emiliano Santarnecchi [a, 1, *]

[a] Precision Neuroscience & Neuromodulation Program, Gordon Center for Medical Imaging, Department of Radiology, Massachusetts General Hospital, Harvard Medical School, Boston, MA, USA
[b] Department of Neuroscience & Padova Neuroscience Center, University of Padova, Padova, Italy
[c] Department of Neuroscience, Imaging and Clinical Sciences, University "G. d'Annunzio", Chieti, Italy
[d] Network Science Institute and Department of Physics, Northeastern University, Boston, MA, USA
[e] Department of Medicine, Brigham and Women's Hospital, Harvard Medical School, Boston, MA, USA
[f] Department of Network and Data Science, Central European University, Budapest, Hungary
[g] Department of Computer Science, University of Calgary, Calgary, AB, Canada
[h] Department of Physics and Astronomy, University of Calgary, Calgary, AB, Canada
[i] Hotchkiss Brain Institute, University of Calgary, Calgary, AB, Canada
[j] Krembil Centre for Neuroinformatics, Centre for Addiction & Mental Health, Toronto, Canada
[k] Alberta Children's Hospital Research Institute, University of Calgary, Calgary, AB, Canada

ARTICLE INFO

Article history:
Received 1 April 2022
Received in revised form
29 July 2022
Accepted 23 September 2022
Available online 14 October 2022

Keywords:
Transcranial magnetic stimulation
Personalized care
Network control theory
Noninvasive brain stimulation

ABSTRACT

Background: In recent years, the possibility to noninvasively interact with the human brain has led to unprecedented diagnostic and therapeutic opportunities. However, the vast majority of approved interventions and approaches still rely on anatomical landmarks and rarely on the individual structure of networks in the brain, drastically reducing the potential efficacy of neuromodulation.
Objective: Here we implemented a target search algorithm leveraging on mathematical tools from Network Control Theory (NCT) and whole brain connectomics analysis. By means of computational simulations, we aimed to identify the optimal stimulation target(s)— at the individual brain level— capable of reaching maximal engagement of the stimulated networks' nodes.
Results: At the model level, in silico predictions suggest that stimulation of NCT-derived cerebral sites might induce significantly higher network engagement, compared to traditionally employed neuromodulation sites, demonstrating NCT to be a useful tool in guiding brain stimulation. Indeed, NCT allows us to computationally model different stimulation scenarios tailored on the individual structural connectivity profiles and initial brain states.
Conclusions: The use of NCT to computationally predict TMS pulse propagation suggests that individualized targeting is crucial for more successful network engagement. Future studies will be needed to verify such prediction in real stimulation scenarios.

1. Introduction

The brain is a complex network, whose components are linked to one another via intricate structural communication pathways. Its organization displays a number of features, such as rich clubs [1], modular hierarchy [2], and an abundance of motifs [3]. This network organization is thought to support a trade-off between physical wiring cost and efficient information propagation [4,5], while also facilitating both localized functional specialization and the rapid global integration of information between different brain regions [6]. This optimized network structure evolves throughout development [6], progressively forming the underlying backbone necessary to support the neural processes responsible for higher order human cognition [7]. Most importantly, the brain's wiring

* Corresponding author. Precision Neuroscience & Neuromodulation Program, Gordon Center for Medical Imaging, Department of Radiology, Massachusetts General Hospital, Harvard Medical School, Boston, MA, USA.
E-mail address: esantarnecchi@mgh.harvard.edu (E. Santarnecchi).
[1] Contributed Equally.

https://doi.org/10.1016/j.brs.2022.09.011

diagram, that is, the connectome, is subject to high levels of interindividual variability, responsible for many of the observed differences in human behavior [8,9]. However, some network alterations are associated with both neurological and psychiatric conditions [6]. Growing interest is therefore being directed towards the possibility of therapeutically manipulating the human functional connectome: carefully altering its activity to a desired state by means of external perturbations. Such interventions are opening a new avenue of selective manipulation of region-to-region connections, or larger networks, leading to behaviorally relevant changes and clinically measurable outcomes [10,11]. For network manipulation to be effective, however, models need to be constructed that are capable of precisely predicting perturbation patterns and outcomes at the individual level. Noninvasive Brain Stimulation (NiBS) covers a wide range of techniques that make use of transcranially applied electrical currents in order to reach cortical layers and promote, or inhibit, neural activity. One of the first and most widely implemented of these approaches is Transcranial Magnetic Stimulation (TMS). In TMS, strong and fast electromagnetic pulses are delivered from a coil positioned on the individual's head. These pulses generate underlying secondary electrical currents capable of causing neural discharges [12]. Thanks to its efficacy and ease of use, TMS is routinely employed in research studies investigating normal brain function, as well as in clinical trials. Furthermore, TMS devices have received clearance from the U.S. Food and Drug Administration (FDA) as a treatment option for medication-resistant Depression [13], Migraine [14] and Obsessive Compulsive Disorder [15].

Nevertheless, major concerns have been raised regarding the high interindividual variability in TMS responses [16,17]. One critical concern is that stimulation targets are often chosen based on fixed anatomical landmarks, reflecting group-level statistics on the role of a specific brain region in a given behavior. Hence, the same brain region is usually selected as the target across all individuals, completely disregarding the interindividual differences in brain structure and underlying network topology that ultimately shape the effect of stimulation. For instance, recent perturbation studies have demonstrated the tight link between network topology and individual cognitive profiles, highlighting the benefits of individualized targeting in ensuring high specificity of the induced perturbation [18]. Indeed, in complex biological networks, knowledge of the network topology is sufficient to predict perturbation patterns with 65–80% accuracy rate, suggesting that topological models might be employed for the investigation of biological interactions [19]. A number of studies have exploited notions from the nascent field of Network Control Theory (NCT) to advance the quest to explain the relationship between network topology and network function [20–23]. Specifically, NCT applied to the brain allows us to query which regions have greater ability to drive the whole brain system towards desired states of activation due to their connectivity profiles [24]. We can also describe the amount of control energy required to favor such state-to-state transitions [20]. The mathematical framework for the study of the effects of externally applied inputs on complex ensembles is at the core of NCT, which particularly suits the modeling of perturbation studies [22,25,26]. Indeed, NCT can be used to reveal trajectories and complex network dynamics considering the interactions between network components [25]. In the present study (Fig. 1), we make use of NCT principles to identify target stimulation sites that activate functional networks in the brain from an individual's structural connectome and their initial functional state. To do so, we compared the effects of different stimulation scenarios in reaching maximum engagement of specific functional networks, targeting: (i) one or two general cortical nodes derived from prior TMS studies (respectively, Trad-1 and Trad-2); (ii) two individualized nodes based on graph theory properties (i.e., two nodes with the shortest path length (PL) or two nodes with the highest weighted nodal degree (ND) to other nodes of the network); (iii) one or two nodes derived from NCT predictions (respectively, NCT-1 and NCT-2). We hypothesized that once we take the individual network topology into account, interindividual variability in optimal stimulation sites will become apparent. For this reason, we also hypothesized that individualized stimulation approaches will have higher chances of reaching network nodes, compared to traditional stimulation approaches. Since NCT sites are optimized to induce the maximum network engagement via our dynamical model, they will necessarily outperform any other stimulation condition. However, if traditional sites already represent efficient stimulations entries for network engagement, then we should observe no significant difference in the models comparing their performance to that of NCT predictions.

2. Methods

2.1. Neuroimaging data and individual connectome extraction

For the purposes of this study, structural and functional neuroimaging data of 400 healthy young individuals (Males = 170; Age range 21–35 years old) were taken from the Human Connectome Project (HCP) Dataset (https://ida.loni.usc.edu) [27]. Of those, 45 participants (Males = 11) underwent neuroimaging data acquisition twice (4.7 ± 2 months interval) for test-retest purposes.

The HCP consortium makes available to the user both diffusion tensor imaging data (DTI) and resting state functional magnetic resonance imaging (rs-fMRI) data that have already undergone basic preprocessing steps [28–31]. On top, spatial smoothing with a kernel with a full width at half maximum of 6 mm and a band-pass filter [0.001–0.080Hz] were also applied to rs-fMRI data to remove potential remaining noise confounds.

As for DWI data, the preprocessing pipeline was run in Ubuntu 18.04 LTS and included tools in FMRIB Software Library (FSL 5.0.3; www.fmrib.ox.ac.uk/fsl) [32], MRtrix3 (www.MRtrix.readthedocs.io) [33] and FreeSurfer [34]. All images downloaded were already corrected for motion via FSL's EDDY [35] following the HCP pipeline [36]. The multi-shell multi-tissue response function [37] was estimated using constrained spherical deconvolution algorithm [38]. Simultaneously, the T1w images, which were already coregistered to the b0 volume, were segmented using FAST algorithm [39]. Anatomically constrained tractography was employed to generate the initial tractogram with 10 million streamlines [40] using second-order integration over fiber orientation distributions [41]. Then, spherical-deconvolution Informed Filtering of Tractograms (SIFT2) methodology [42] was applied in order to provide more biologically accurate measures of fiber connectivity.

As for the atlas, an ad-hoc brain parcellation of 226 regions of interest (ROIs) covering cortical, subcortical and cerebellar structures was extrapolated and then used to extract highly individualized connectomes. Specifically, for our cortical ROIs, the Schaefer Atlas of 200 parcels [43], which distinguishes into 7 functional networks (Visual- VIS, Sensorimotor- SMN, Dorsal Attention- DAN, Ventral Attention- VAN, Limbic- LIMB, Frontoparietal- FPN, Default Mode- DMN), was mapped to the individual's FreeSurfer parcellation using spherical registration [44]. A distinction into the same networks was also applied for 14 cerebellar ROIs, which were extracted from the Buckner Atlas [45]. Furthermore, a Freesurfer parcellation was ultimately applied to derive individual ROIs of 12 subcortical structures, including the bilateral basal ganglia (divided into the putamen, caudate and pallidum nuclei), the amygdalae and thalami. As a result, 226x226 connectivity matrices were extracted, representing the number of white matter tracts connecting each

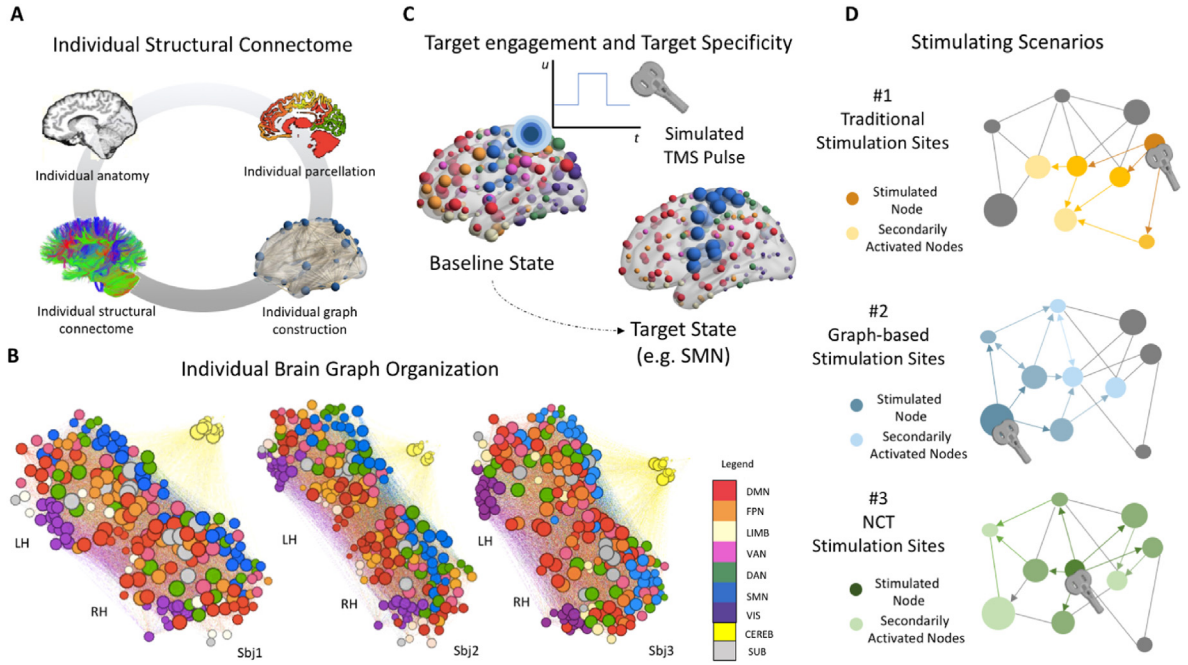

Fig. 1. Methodological workflow. A. Individual subject anatomy and diffusion tensor imaging (DTI) data were employed for the construction of individual cortical, subcortical and cerebellar parcellations into a total of 226 regions. Individual graphs were then built, in which brain regions are nodes and their structural connections are edges. **B.** Interindividual differences in the brain graph organization are shown for 3 exemplificative individuals. Although a general structure is common across participants (i.e., the division of the graph into 2 distinct hemispheres and the cerebellum), differences can be observed in the layout of the single nodes forming the cerebral networks. **C.** Simulations of cortical activation patterns following the delivery of a TMS pulse were run. NCT was applied to determine the best simulating scenario for the transitioning of brain activity from an initial state to a desired final state, here represented by the marked activation of the SMN (blue dots). **D.** Three different stimulating scenarios were compared in their efficacy to induce targeted network engagement. Specifically, we compared the efficacy of stimulation applied to i) traditional stimulation sites, as found in the literature; ii) stimulation sites that were derived from graph theory analysis, namely nodes with the shortest path length or with the highest nodal degree to the rest of the network nodes; iii) sites from NCT predictions, that is, nodes that have the greatest success of driving the system toward a desired final state. We hypothesize that different stimulation scenarios will result in different activation patterns in the surrounding nodes as a function of their connectivity and distance to the stimulation site.
CEREB= Cerebellar; DAN = Dorsal Attention Network; DMN = Default Mode Network; FPN= Frontoparietal Network; LH = Left Hemisphere; LIMB = Limbic Network; NCT= Network Control Theory; RH = Right Hemisphere; Sbj = Subjects; SMN= Sensorimotor Network; SUB= Subcortical; TMS = Transcranial Magnetic Stimulation; VAN= Ventral Attention Network; VIS= Visual Network.

pair of ROIs. The same ROIs were used to extract changes in the fluctuations of the Blood Oxygen Level Dependent (BOLD) signal, which was used to inform the model about the baseline state of activity prior to stimulation. The final connectivity matrices were also normalized based on the size of each ROIs [46]. Based on the principles of Graph Theory, we used graphs to represent the individual structural connectome, whereby brain regions are treated as nodes and their structural connections as edges [47] (Fig. 1 A, B). The use of a graph to represent the brain connectome is crucial in order to study the individual pathways of information flow.

2.2. Network control theory for stimulation target selection

To determine the efficacy of different targeting scenarios, we constructed a model to simulate the transition from an initial state to a desired target state following the application of an external input, mimicking a TMS pulse (Fig. 1C). Consistent with prior literature, we assumed the linear time-invariant network dynamics described by:

$$\dot{x}(t) = Ax(0) + Bu(t) \quad (1)$$

where A is a nxn matrix that represents the individual structural connectome and $x(0)$ is the $nx1$ vector of activity of each brain region, as measured by BOLD activity. We define $x(0)$ to be the individual initial state extracted from the timeseries of the participant's resting-state fMRI at the first time point of scanning. To prevent uncontrolled trajectories, A was stabilized by dividing the matrix by its biggest eigenvalue and then by multiplying it by a fixed constant. We denote the external input (u), which has the form of a simple pulse, and specify which nodes u is applied to via B, an nxn adjacency matrix (Fig. 2A). B(i,i) = 1 if u is applied to node i. The efficacy of a model's prediction was then determined based on the vicinity of the simulated final state to the desired final state. We defined the desired final state as having maximal activity in the nodes belonging to the network of interest. In other words, the desired final state is defined by the experimenter and it represents a condition of maximum activity in an ensemble of nodes forming a network. For example, a researcher or clinician might wish to activate the nodes belonging to the DMN. In this scenario, the desired final state is hence a condition of maximum activity in the DMN. That is, any brain-wide activity levels that involved a greater activation of nodes in the DMN as compared to nodes in other subnetworks. Specifically, we assessed the efficacy of the model by considering the number of the most highly activated nodes that lie in the network of interest. Specifically, we calculated:

$$I \cap S_{net} = \{i : i \in I \text{ and } i \in S_{net}\} \quad (2)$$

where I is the set of the top 30 nodes (roughly 10%) as ranked by their activation levels following stimulation and S is the set of nodes in the network of interest. Results at different values of I (e.g., 15% or 40%) are available in the Supplementary Materials and prove consistency across thresholds. To go back to our example, if we want to reach a state of DMN activity, then our desired final state is that with maximum activity in the nodes of the DMN and S_{net} is the set

of nodes in the DMN. A trajectory that successfully reaches this desired final state will result in greater activation of DMN nodes compared to nodes belonging to other resting state networks. In other words, the most effective stimulation scenario will increase vicinity to the desired target state, in the sense that it will mostly result in activation of the nodes belonging to the network we wish to reach (i.e., the target state) and it will do so by inducing the greatest activity in such nodes (i.e., they will be the nodes showing the greatest change in activity compared to baseline). For the purposes of the present study, the trajectories arising from 3 different stimulation scenarios were compared in their efficacy to reach a desired final state (Fig. 2A). The first of those trajectories was represented by the stimulation of *traditional* stimulation sites, where commonly employed TMS literature targets were used as input nodes. Our second trajectories were *graph* derived, whereby input nodes were chosen as the nodes with the shortest path length or the highest nodal degree to the other nodes in the network, as those are two of the most common graph properties underlying information exchange between nodes. We define the weighted path length of a specific node i to a given network S_{net} as:

$$d_{i,S_{net}} = \sum_{j \in S_{net}} w_{ij} \tag{3}$$

where w is the non-zero weighted shortest path length from node i to node j [47]. That is, we simply sum path lengths from i to all nodes j in the network of interest. Note that we take the reciprocal of edge weights when calculating short path lengths to ensure that the higher weight of a stronger connection is reflected as a shorter path through the network. The network-specific measure of weighted nodal degree was then computed as the total sum of the weighted links connecting a given node to all other nodes of the network of interest. The Brain Connectivity Toolbox (https://sites.google.com/site/bctnet/) function running in MATLAB 2017b was used to extract these graph theory parameters.

Finally, our third stimulation condition was based on our *Network Control Theory* predictions. As described above, the dynamics described in equation (1) were simulated. We iteratively applied the input signal to all nodes in the parcellation to identify the most efficient stimulation target. We chose the stimulation target retrospectively as the one that activates the highest number of nodes belonging to the target state of interest within the first 10% of the activated nodes overall. As a result, our simulations could either target the same stimulation site for all our subjects (trad), or they could vary based on two degrees of personalization: graph-based (PL and ND) and NCT (Fig. 2B).

Finally, prior work has highlighted the issue that in order to guide a system to desired states, the number of nodes stimulated has to be relatively high (16%–25% of all nodes) [23]. However, current TMS approaches can enable the application of not more than two stimulation targets simultaneously by means of double coil use, also known as cortico-cortical paired associative stimulation [48]. For these reasons, we also compared the efficacy of targeting 1 node versus targeting 2 nodes, defined as i) the second most common TMS target in prior literature studies, ii) the second node with the shortest path length or highest weighted nodal degree to the network of interest, iii) the second node reaching maximum network engagement according to NCT predictions.

Importantly, we implemented a model based on linear dynamics [22,49]. The assumption of linearity does not accurately reflect neuronal dynamics, which are inherently nonlinear in most processes. However, studies have shown that linear models can account for a significant amount of the variation in brain activity as

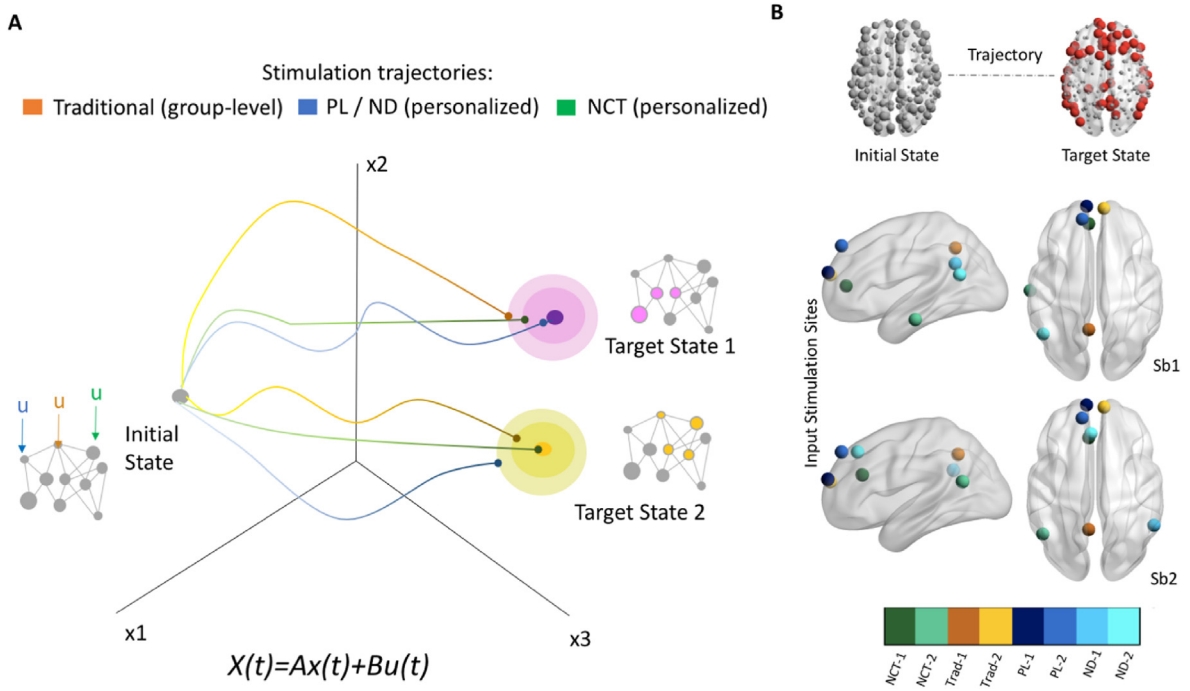

Fig. 2. Theoretical Background and Applications. A. NCT is a mathematical approach for the study of the controllability of dynamical systems. NCT queries our ability to drive a system from any initial state to any desired final state in finite time via the application of suitable input signals. Different transitioning trajectories can be realized depending on the target site, the input signal, and the state space. A more efficient trajectory is characterized by less control energy and a more direct path, which ultimately brings the system closer to the desired state. **B.** In our simulations, the input sites could be equal for all subjects, based on literature-derived sites of stimulation, or they could be personalized based on: a graph theory approach selecting the nodes with the shortest path length or the highest nodal degree to the other nodes of the network; or based on data-driven NCT predictions of the best stimulation sites for each subject.

measured by fMRI [50]. Linear dynamics can successfully approximate the full nonlinear system locally. Indeed, if a system is locally controllable along a specific trajectory in the state space, then the corresponding nonlinear system is also controllable along the same trajectory [51]. Simulations have demonstrated that predictions from linear control are consistent with neuronal networks with Wilson-Cowan nonlinear dynamics [52], and that the nonlinear controllability of motifs with non-identical link weights exhibits the same properties as its linear and structural counterpart [53]. Furthermore, a recent study assessed the ability of various linear and nonlinear models to capture macroscopic brain dynamics, and came to the surprising conclusion that linear approaches outperform the nonlinear models in terms of predictive power, computational complexity, and the extent of residual dynamics unexplained by the model [54]. This may be due in part to microscopic dynamics being masked at the macroscopic level by averaging over space and time. Network control approaches in the human brain continue to produce results derived from the assumption of linearity that are relevant to and consistent with brain dynamics and behaviour [20–22,55–58].

Overall, we compared the ability of the aforementioned in silico stimulation scenarios to target each resting-state network (VIS, SMN, DAN, VAN, LIMB, FPN and DMN), as well as two networks of high clinical and experimental relevance. In this regard, a term-based meta-analytic search by means of Neurosynth (https://neurosynth.org/) was conducted to derive the activation map of the cerebral areas most often associated across studies on Depression (key term: “depression”), as well as an activation map of the areas underlying Cognitive Control (key term: “cognitive control”), whose dysfunction is often targeted in stimulation protocols for both depression [59] and other psychiatric conditions, such as obsessive compulsive disorder [60].

For our statistical tests, within-subject repeated measures analyses of variance (ANOVAs) were run in MATLAB 2017b to control for significant differences across the 9 stimulation conditions, targeting: i) two commonly employed target sites according to the literature, either in isolation or simultaneously (respectively named trad-1 and trad-2); ii) the stimulation of two path length-derived nodes (PL); iii) the stimulation of two nodes with the highest nodal degree (ND); iv) and the targeting of either one or two nodes based on NCT predictions (NCT-1 and NCT-2) (Fig. 2B). As a result, we always compared the effect of stimulating multiple nodes (i.e., two) across all conditions (traditional, graph-derived, NCT-derived) to ensure that benefit of one stimulation scenario over the others did not simply arise from having multiple stimulated sites. In addition, in order to control for possible effects of networks' topology and spatial proximity, we further compared the effect of stimulation of two types of randomly rewired networks: (i) preserving weight, degree, and strength distribution (Topological Null Model-TN); and (ii) preserving the relationship of weight and distance between nodes (Spatial Null Model-SN). TN models have the advantage of maintaining the degree distribution whilst reshuffling network structure, whereas SN models retain the strength-distance relationship observed in spatial brain networks and shuffle the network's topological structure [61,62]. TN models were constructed by means of the Brain Connectivity Toolbox [47], whereas SN models were constructed based on the available code from Roberts et al., 2016 [62] as previously reported in the literature [22].

Post-hoc comparisons were then run to specifically look at each single contrast in our model. A significant threshold of $\alpha = 0.05$ was used to reject the null hypothesis and Bonferroni correction was applied to control for multiple comparisons.

3. Results

3.1. Network engagement

We tested the use of NCT predictions to identify sites of stimulation for 7 functional networks (VIS, SMN, DAN, VAN, LIMB, FPN, DMN) according to the Schaefer Atlas parcellation [43]. To control for possible effects of networks' topology and spatial proximity, we further compared the effect of stimulation of two types of randomly rewired networks (TN and SN). For all networks tested, all in silico stimulations always resulted in a significantly lower amount of activated nodes compared to the individualized stimulation based on NCT predictions. An example of the typical trajectories of activated nodes is reported in Fig. 3 for the DMN, where the sequence of activated nodes is shown for one exemplificative subject following the stimulation the NCT target (propagation outreach for the other conditions is shown in Fig. S1 in the Supplementary Materials). All four approaches successfully activate nodes belonging to the DMN; however, the NCT approach displays the highest specificity in the activation of DMN nodes compared to the activation of nodes belonging to any other brain network (Fig. 3D). Furthermore, in accordance with prior literature, stimulation of two nodes always resulted in greater network activation compared to targeting only a single node (Fig. 3C). Altogether, targeting of the DMN showed at least one significant difference between conditions ($F_{(8,3192)} = 2159.7$, $p < 0.0001$). Subsequent post-hoc comparisons revealed that targeting of traditional stimulation sites, such as the left precuneus [63,64](PC-l) ($M_{PC\text{-}l} = 11.02$, $SD_{PC\text{-}l} = 1.63$; $p < 0.0001$); the right medial prefrontal cortex [64](PFC-r) ($M_{PFC\text{-}r} = 14.06$, $SD_{PFC\text{-}r} = 1.2$; $p < 0.0001$); or of both sites simultaneously ($M_{PC\text{-}l\ +\ PFC\text{-}r} = 14.28$, $SD_{PC\text{-}l\ +\ PFC\text{-}r} = 1.24$; $p < 0.0001$) activated fewer nodes compared to our NCT-2 approach ($M_{NCT} = 18.71$; $SD_{NCT} = 1.19$). Similarly, network topological measures alone were not able to reach the levels of DMN activation achieved by NCT ($M_{PL} = 15.68$, $SD_{PL} = 1.41$, $p < 0.0001$; $M_{ND} = 14.9$, $SD_{ND} = 2.18$, $p < 0.0001$), nor were the TN ($M_{TN} = 6.95$, $SD_{TN} = 2.05$; $p < 0.0001$) and SN models ($M_{SN} = 14.2$, $SD_{SN} = 1.78$; $p < 0.0001$) (Fig. 3C).

For the LIMB network, the model showed at least one significant difference between our conditions ($F_{(8,3192)} = 4102.5$, $p < 0.0001$). Subsequent post-hoc comparisons revealed that the targeting of traditional stimulation sites, that is, the dorsolateral prefrontal cortex for the left and right hemispheres [65,66] (DLPFC-l and DLPFC-r) ($M_{DLPFC\text{-}l} = 1$, $SD_{DLPFC\text{-}l} = 0.34$; $p=<0.0001$; $M_{DLPFC\text{-}r} = 0.71$, $SD_{DLPFC\text{-}r} = 0.58$; $p=<0.0001$), as well as the targeting of both sites simultaneously ($M_{DLPFC\text{-}l\ +\ DLPFC\text{-}r} = 0.79$, $SD_{DLPFC\text{-}l\ +\ DLPFC\text{-}r} = 0.40$; $p < 0.0001$) resulted in significantly fewer activated nodes compared to our NCT-2 approach ($M_{NCT} = 8.48$, $SD_{NCT} = 1.05$). Stimulation based on PL ($M_{PL} = 5.6$, $SD_{PL} = 1.13$; $p < 0.0001$) or ND ($M_{ND} = 4.68$, $SD_{ND} = 1.33$; $p < 0.0001$) also resulted in a smaller number of activated nodes, similar to what happened with the stimulation of TN ($M_{TN} = 2.57$, $SD_{TN} = 0.9$; $p < 0.0001$) and SN ($M_{SN} = 7.86$, $SD_{SN} = 1.85$; $p < 0.0001$) models. In regard of the FPN, the model showed at least one significant difference between our conditions ($F_{(8,3192)} = 1336.6$, $p < 0.0001$). Subsequent post-hoc comparisons revealed that stimulating the left superior parietal lobule (SPL-l) or the PFC-r [67,68]($M_{SPL\text{-}l} = 4.89$, $SD_{SPL\text{-}l} = 0.97$, $p < 0.0001$; $M_{PFC\text{-}r} = 8.35$, $SD_{PFC\text{-}r} = 1.77$; $p < 0.0001$), or stimulating both sites simultaneously

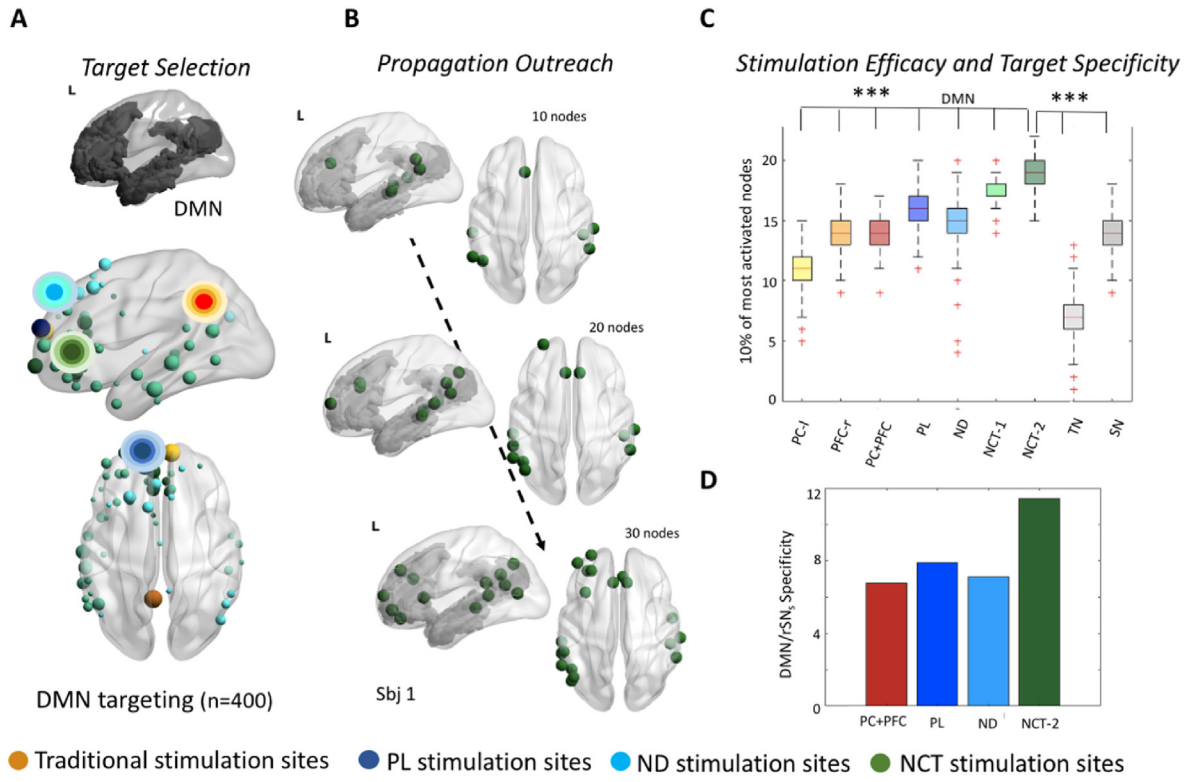

Fig. 3. Propagation outreach and network engagement. A. Target selection based on group-level data (trad) versus personalized stimulation sites (PL, ND and NCT) is shown for the DMN stimulation. Trad sites are common across all subjects, whereas PL, ND and NCT showed great interindividual variability across the 400 individuals analyzed in this study. The size of the dot is proportional to the number of subjects sharing the same stimulation node. The most popular stimulation site for all conditions is highlighted. **B.** Propagation outreach following NCT stimulation in an exemplificative subject. As shown in reference to the DMN template, stimulation of the individual NCT node shows selective activation of DMN nodes. **C.** The efficacy of different stimulation scenarios is shown as a boxplot. Overall, the simultaneous stimulation of 2 sites derived from NCT predictions significantly recruited a higher number of DMN nodes compared to all other approaches. **D.** The achieved network specificity following each stimulation condition is shown, averaged across individuals. The number of activated nodes belonging to the DMN compared to the number of activated nodes belonging to any other resting state network (rSNs) was highest for the NCT condition, suggesting higher specificity.
***$p < 0.001$.

($M_{SPL + PFC} = 7.48$, $SD_{SPL + PFC} = 1.23$; $p < 0.0001$) resulted in fewer activated nodes compared to our NCT-2 approach ($M_{NCT} = 13.04$, $SD_{NCT} = 1$). Stimulation based on PL ($M_{PL} = 8.87$, $SD_{PL} = 2.31$; $p < 0.0001$), ND ($M_{ND} = 9.82$, $SD_{ND} = 1.93$; $p < 0.0001$), TN and SN models ($M_{TN} = 4.91$, $SD_{TN} = 1.88$; $p < 0.0001$; $M_{SN} = 9.64$, $SD_{SN} = 1.69$; $p < 0.0001$) also resulted in fewer activated nodes compared to NCT-2. As for the DAN, the model showed at least one significant difference between our conditions ($F_{(8,3192)} = 1907.8$, $p < 0.0001$). Subsequent post-hoc comparisons revealed that stimulation of SPL-l and of the right inferior frontal gyrus (IFG-r) [69]($M_{SPL-l} = 7.43$, $SD_{SPL-l} = 1.1$; $p < 0.0001$; $M_{IFG-r} = 4.97$, $SD_{IFG-r} = 1.15$; $p < 0.0001$), of both sites simultaneously ($M_{SPL + IFG} = 7.3$, $SD_{SPL + IFG} = 1.47$; $p < 0.0001$), PL ($M_{PL} = 12.18$, $SD_{PL} = 1.73$; $p < 0.0001$), ND ($M_{ND} = 12.15$, $SD_{PL} = 2.15$; $p < 0.0001$), TN and SN models ($M_{TN} = 5.15$, $SD_{TN} = 1.75$; $p < 0.0001$; $M_{SN} = 11.45$, $SD_{SN} = 2.08$; $p < 0.0001$) resulted in fewer activated nodes compared to our NCT-2 approach ($M_{NCT} = 14.82$, $SD_{NCT} = 1.87$). In regards to SMN stimulation, the model showed at least one significant difference between our conditions ($F_{(8,3192)} = 1791.9$, $p < 0.0001$). Subsequent post-hoc comparisons revealed that stimulation of the left and right primary motor cortices (M1) [70] ($M_{M1-l} = 13.53$, $SD_{M1-l} = 1.48$, $p < 0.0001$; $M_{M1-r} = 14.83$, $SD_{M1-r} = 1.59$; $p < 0.0001$), of both sites simultaneously ($M_{M1-l + M1-r} = 17.96$, $SD_{M1-l + M1-r} = 1.33$; $p < 0.0001$), PL ($M_{PL} = 14.79$, $SD_{PL} = 1.74$; $p < 0.0001$) and ND ($M_{ND} = 15.8$, $SD_{ND} = 2.03$; $p < 0.0001$) conditions, TN and SN models ($M_{TN} = 5.80$, $SD_{TN} = 1.78$; $p < 0.0001$; $M_{SN} = 13.74$, $SD_{SN} = 3.76$; $p < 0.0001$) resulted in fewer activated nodes compared to our NCT-2 approach ($M_{NCT} = 19.14$, $SD_{NCT} = 1.26$). For the VIS network, the model showed at least one significant difference between our conditions ($F_{(8,3192)} = 2738$, $p < 0.0001$). Subsequent post-hoc comparisons revealed that stimulation of the primary visual cortex for the left or right hemispheres in isolation (O1 and O2) [71] ($M_{o1} = 16.14$, $SD_{o1} = 2.06$; $p < 0.0001$; $M_{o2} = 17.26$, $SD_{o2} = 1.69$; $p < 0.0001$) or of both sites simultaneously ($M_{o1+02} = 23.1$, $SD_{o1+02} = 1.28$; $p < 0.0001$) resulted in fewer activated nodes compared to our NCT-2 approach ($M_{NCT} = 23.68$, $SD_{NCT} = 1.3$). Similarly, stimulation based on PL ($M_{PL} = 18.93$, $SD_{PL} = 2.96$; $p < 0.0001$), ND ($M_{ND} = 21.64$, $SD_{ND} = 3.16$; $p < 0.0001$), TN and SN models ($M_{TN} = 7.17$, $SD_{TN} = 2.15$; $p < 0.0001$; $M_{SN} = 21.74$, $SD_{SN} = 2.3$; $p < 0.0001$) also resulted in fewer activated nodes compared to NCT-2. Finally, for the in-silico prediction of VAN stimulation, the model showed at least one significant difference between our conditions ($F_{(8,3192)} = 1688.1$, $p < 0.0001$). Subsequent post-hoc comparisons revealed that stimulation of the right temporo-parietal junction (TPJ-r) or of the right middle frontal gyrus (MFG-r) [72] ($M_{TPJ-r} = 6.06$, $SD_{TPJ-r} = 0.9$, $p < 0.0001$; $M_{MFG-r} = 3.7$, $SD_{MFG-r} = 0.87$; $p < 0.0001$), of both sites simultaneously ($M_{TPJ + MFG} = 6.55$, $SD_{TPJ + MFG} = 0.9$; $p < 0.0001$), PL ($M_{PL} = 6.55$, $SD_{PL} = 0.99$; $p < 0.0001$), ND ($M_{ND} = 6.36$, $SD_{ND} = 1.43$; $p < 0.0001$), TN and SN models ($M_{TN} = 3.55$, $SD_{TN} = 1.55$; $p < 0.0001$; $M_{SN} = 6.94$, $SD_{SN} = 1.3$; $p < 0.0001$) resulted in fewer activated nodes compared to our NCT-2 approach ($M_{NCT} = 10.65$, $SD_{NCT} = 0.98$). All the reported results survived Bonferroni's

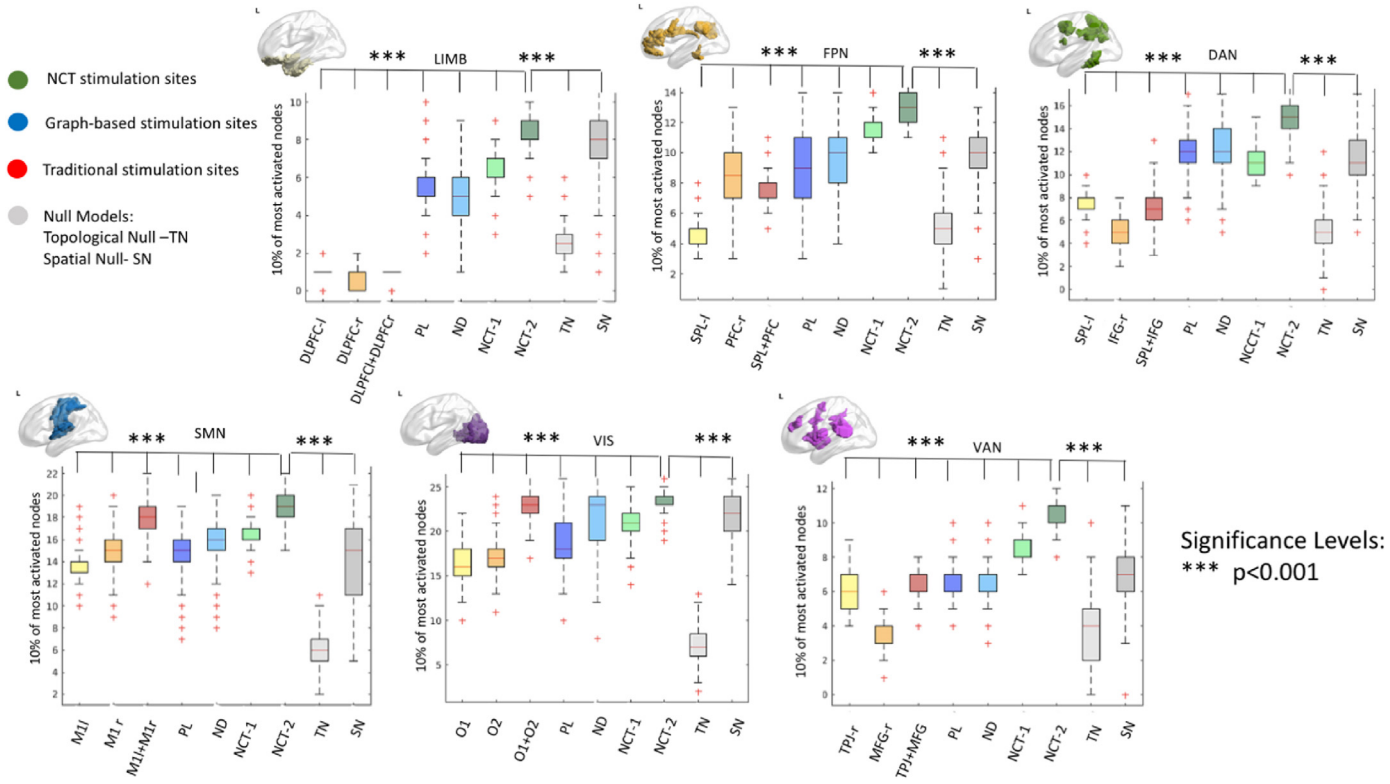

Fig. 4. Statistical comparisons of the efficacy of stimulating scenarios and their controls. Efficacy of the different stimulation approaches was computed by looking at how many nodes, within the first 10%, belonged to the network of interest following the stimulation. Across all the stimulated networks, we observed that the simultaneous stimulation of 2 nodes always induced greater network engagement than the stimulation of a single node. For all the networks tested, the stimulation of 2 nodes derived from NCT predictions always resulted in a greater number of nodes activated with respect to Trad, PL and ND conditions. Stimulation of topological and spatial null models was also run, to control for the effects of topology and spatial proximity of the nodes in guiding the effect of the simulations.

correction for multiple comparisons. The full list of contrasts with the corrected p-values can be found in the Supplementary Table S1. Boxplots for each network stimulation scenarios are reported in Fig. 4.

3.2. Network specificity

To control for the specificity of our NCT stimulation scenarios, we computed the amount of activation of nodes belonging to the network of interest compared to the activation of nodes belonging to other resting-state networks (Fig. 5). Overall, we observed that specificity for targeting the DMN was high, with higher activation (91%) for nodes belonging to the DMN and the remaining percentage of activated nodes belonging mostly to the FPN (6.23%) and LIMB (1.23%) networks. Targeting of the FPN also resulted in 78.83% of target specificity, with less activation of nodes belonging to the VAN (13.11%) and DMN (6.74%) networks. VIS network targeting reached the highest specificity, with 98.4% activation of nodes belonging to the VIS network and the remaining 0.76% to the DMN instead. Stimulation of the LIMB network also reached an 83.55% specificity, with less activation of nodes belonging to the DMN (13.12%) and FPN (1.67%) instead. As for the SMN, its targeting resulted in 59.22% activation of its nodes and 39% activation of nodes belonging to the DAN instead. Similarly, stimulation of the DAN resulted in 57.67% activation of DAN nodes, 23.64% activation of FPN nodes and 14.93% activation of SMN nodes. Finally, VAN stimulation resulted to be the least specific (46.12%), with many of the activated nodes belonging to the SMN (33.48%) and to the DMN (13.84%). A mean average Pearson's correlational matrix was computed, looking at the amount of shared white matter fibers connecting all networks (Fig. 5). High correlational values were observed for the white matter bundles connecting the SMN, VAN and DAN networks ($r_{SMN \leftrightarrow DAN} = 0.90$; $r_{SMN \leftrightarrow VAN} = 0.4$, $r_{DAN \leftrightarrow VAN} = 0.31$), as well as between the DMN and FPN ($r_{DMN \leftrightarrow FPN} = 0.47$), which could explain the tendency of such networks' nodes to co-activate.

3.3. Targeting hot-spots of clinical and research relevance

To test the efficacy of NCT predictions applied on non-resting state networks, we derived meta-analytic maps from studies on Depression and Cognitive Control. These activation maps were used as target in our simulations to determine if NCT predictions could provide insight on targeting of widespread cortical regions that are the ongoing focus of several TMS trials on both patients and healthy participants. For both scenarios, a significant difference was reported across conditions (Depression: $F_{(8,3192)} = 1629.2$, $p < 0.0001$, Cognitive Control: $F_{(8,3192)} = 1687.6$, $p < 0.0001$). The number of cerebral areas commonly reported across studies on Depression (Fig. 6) that we were able to reach in this in silico stimulations was smaller following traditional stimulation of the DLPFC-l or of the right dorsomedial prefrontal cortex (DMPFC-r) [73] ($M_{DLPFC-l} = 6.58$, $SD_{DLPFC-l} = 1.25$; $p < 0.0001$; $M_{DMPFC-r} = 8.16$, $SD_{DMPFC-r} = 1.32$; $p < 0.0001$), of both sites simultaneously ($M_{DLPFC + DMPFC} = 8.49$, $SD_{DLPFC + DMPFC} = 0.97$; $p < 0.0001$), of PL ($M_{PL} = 10.27$, $SD_{PL} = 1.87$; $p < 0.0001$) or ND ($M_{ND} = 7.75$, $SD_{ND} = 2.26$; $p < 0.0001$) sites, TN and SN models ($M_{TN} = 4.39$, $SD_{TN} = 1.76$; $p < 0.0001$; $M_{SN} = 12.73$, $SD_{SN} = 2.25$; $p < 0.0001$) compared to the number of sites we could reach with NCT-2 targets ($M_{NCT} = 13.71$, $SD_{NCT} = 1.05$).

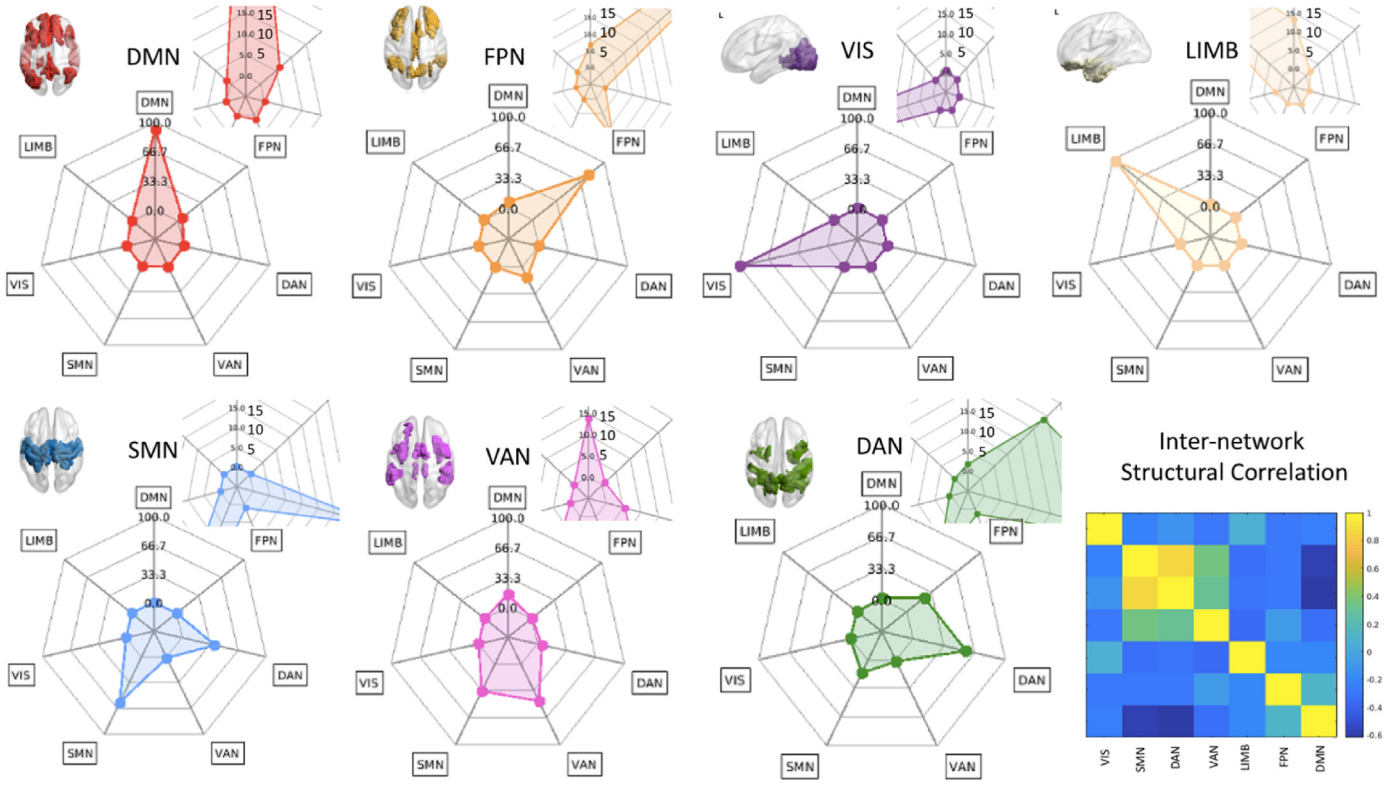

Fig. 5. Target Engagement Specificity. To control for the specificity of our stimulations, we computed the amount of network activation that was specific for the targeted network compared to all other networks in the brain. Following the stimulation of our NCT-derived sites, the engagement of the targeted network was significantly greater than the recruitment of other brain networks. The mean average correlational matrix shows high inter-network connectivity between the SMN, DAN and VAN, thus explaining their tendency to co-activate.

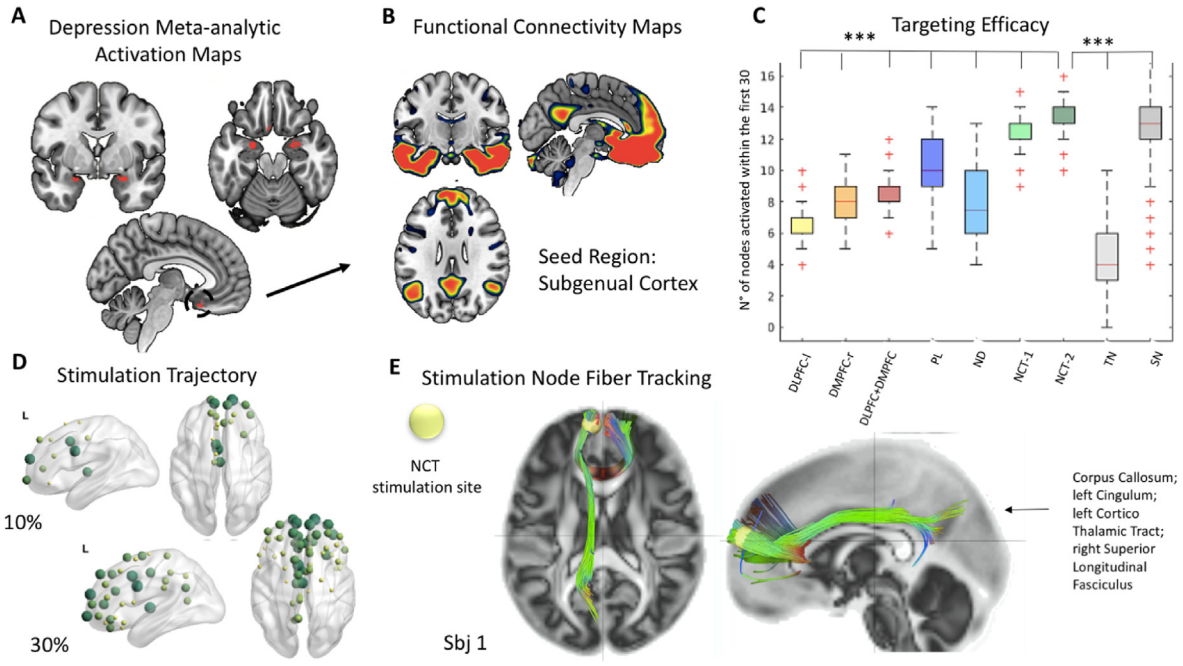

Fig. 6. Depression. A. A meta-analytic search was conducted to derive commonly reported areas across literature studies in major Depression. **B.** The subgenual cortex was taken as seed to show the average connectivity profile with the rest of the brain. **C.** Boxplot of the targeting efficacy of each stimulation condition is shown. **D.** Mean average propagation pathways following NCT stimulation. **E.** Fiber tracts passing through NCT stimulation for one individual are shown (in order: Corpus Callosum; left Cingulum; left Cortico Thalamic Tract; right Superior Longitudinal Fasciculus).

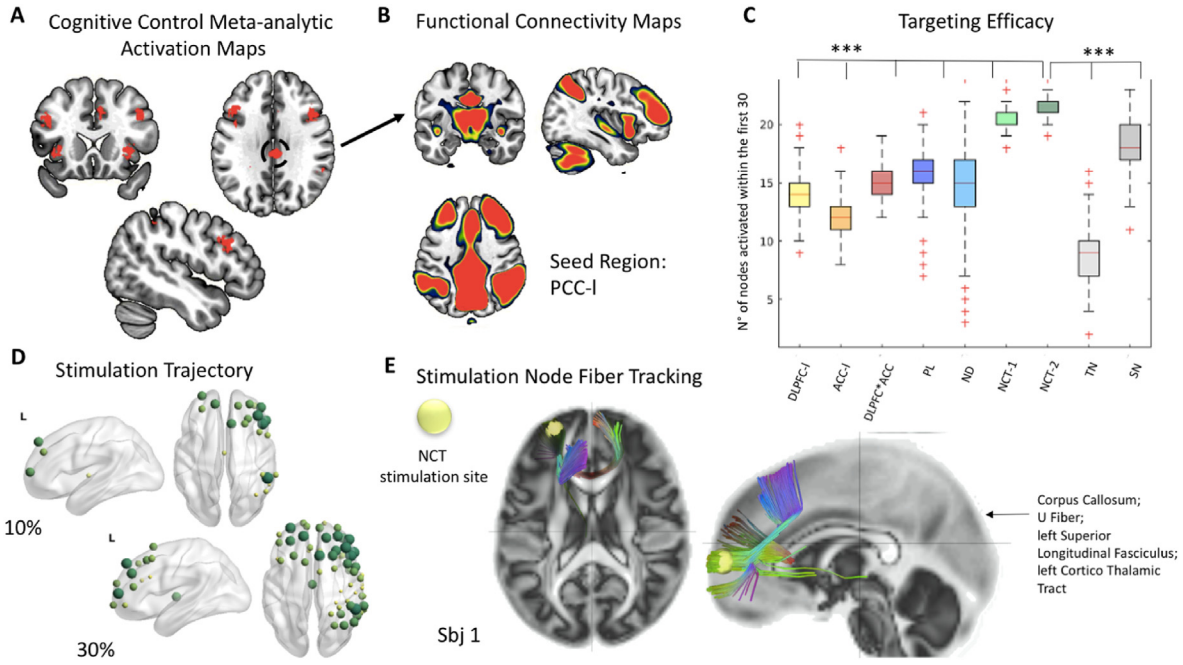

Fig. 7. Cognitive Control. A. A meta-analytic search was conducted to derive commonly reported areas across literature studies on Cognitive Control. **B.** The left posterior cingulate cortex (PCC-l) was taken as seed to show the average connectivity profile with the rest of the brain. **C.** Boxplot of the targeting efficacy of each stimulation condition is shown. **D.** Mean average propagation pathways following NCT stimulation. **E.** Fiber tracts passing through NCT stimulation for one subject are shown (in order, Corpus Callosum; U Fiber; left Superior Longitudinal Fasciculus; left Cortico Thalamic Tract).

Similarly, reaching of Cognitive Control-related regions (Fig. 7) was achieved less following stimulation of the DLPFC-l ($M_{DLPFC-l} = 13.78$, $SD_{DLPFC-l} = 1.7$; $p < 0.0001$) or of the left Anterior Cingulate Cortex (ACC-l) [60] ($M_{ACC-l} = 11.75$, $SD_{ACC-l} = 1.49$, $p < 0.0001$), of both sites simultaneously ($M_{DLPFC + ACC} = 15.1$, $SD_{DLPFC + ACC} = 1.16$; $p < 0.0001$), of PL sites ($M_{PL} = 16.19$, $SD_{PL} = 1.87$; $p < 0.0001$), ND sites ($M_{ND} = 14.36$, $SD_{ND} = 4.16$; $p < 0.0001$), or of TN and SN models ($M_{TN} = 8.93$, $SD_{TN} = 2.14$; $p < 0.0001$; $M_{SN} = 18.35$, $SD_{SN} = 1.75$; $p < 0.0001$) compared to the number of activated nodes by NCT-2 ($M_{NCT} = 21.62$, $SD_{NCT} = 1.08$). All the reported results survived Bonferroni's correction for multiple comparisons. The full list of contrasts with the corrected p-values can be found in the Supplementary Table S1.

In accordance with the notion that cerebral signals travel along structural connections, the mean path of propagation following NCT sites stimulation were observed to overlie with connectivity bundles originating from the targeted node (Fig. 6 D, E; Fig. 7 D, E).

3.4. Personalization of stimulation and test-retest reliability

One of the main objectives of this study was to compare the efficacy of in silico stimulation scenarios tailored at the individual level, compared to group-derived stimulation sites derived from traditional stimulation paradigms in the literature. In this regard, and as hypothesized, great interindividual differences were observed in the optimal NCT stimulation site capable of maximizing network activity, with consequently great interindividual differences in the recruited white matter bundles (Fig. 8).

Within the HCP sample, 45 participants underwent twice the acquisition of DTI and fMRI data at 4.7 ± 2 months interval for test-retest purposes. As such, we were able to determine the reliability of our in silico simulations by looking at the Pearson's correlation between the average number of nodes activated per condition in each visit. As observed in Fig. 9, high test-retest reliability was observed for all TMS simulations. Indeed, across all networks tested, the average number of nodes activated by each stimulation condition was highly consistent across visits. The boxplot reporting the mean and SD for each retest condition in every network tested is reported in the Supplementary Material (Fig. S2).

4. Discussion

In the present study, we tested if NCT could be employed for the identification of nodes capable of guiding the brain network from an initial state toward a desired final state. In this regard, topological models have been proven to be highly predictive of perturbation patterns [19] and hence there is sufficient rationale to believe they could be employed for individualized target selection. In the brain, electrical inputs are known to travel along the structural connections of white matter tracts linking brain regions [75]. As such, models aware of the underlying communication pathways that support information transfer in the brain are likely to provide a more informed guess on the optimal starting point to reach desired brain areas or states [24]. Our findings corroborate this notion proving that the level of network activation following the stimulation of traditional or control sites is lower than what observed when NCT-derived sites are chosen as input, at least in these in silico scenarios. Secondarily, our models predict that the use of two input nodes, compared to the use of a single input node, holds higher chances of engaging more nodes of interest. The use of multiple target nodes over a single one has already been addressed in controllability studies, which claim that at least 16%–25% of nodes should be used to exert complete control on a complex dynamical system like the brain [23]. It is therefore not surprising that we find two nodes outperform one node when we consider stimulation pathways to functional networks in the brain. To ensure the direct relevance of our results to TMS studies, we chose not to test the effects of stimulating more than two regions simultaneously. Indeed, at present, dual coil studies represent the only condition whereby multiple cortical sites are stimulated via

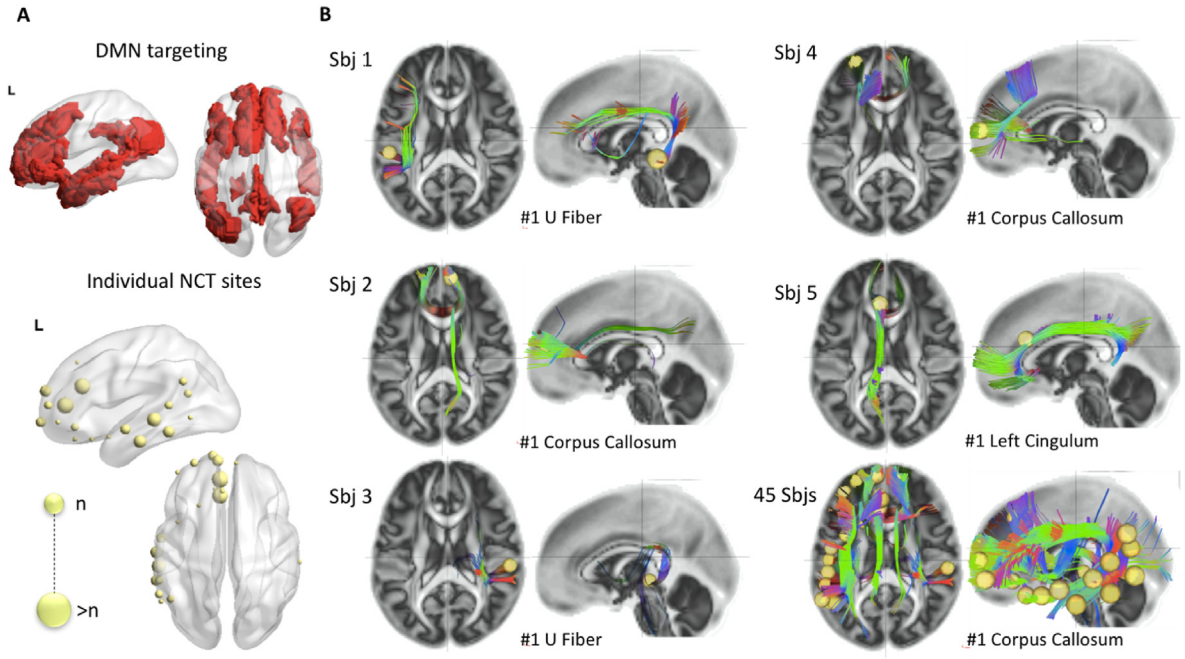

Fig. 8. Personalized Target Selection. A. NCT approaches allow to identify highly personalized stimulation sites that ultimately maximize individual network engagement (e.g., DMN network engagement). The size of the dots is proportional to the number of subjects sharing the same NCT stimulation site. **B.** The HCP tractography atlas [74] was used to perform automatic fibers tracking and labeling. Five exemplificative subjects are shown, revealing the structural paths underlying the individual sites of stimulation, followed by 45 subjects' cumulative tractogram from the test-retest sample. The most prominent structural tract underlying stimulation sites is reported.

TMS, also known as cortico-cortical paired associative stimulation [76]. Although they have been proven efficient in targeting specific cortical networks and promoting specific behaviors [48,77], dual coil approaches are not as often employed as single coil ones, as the

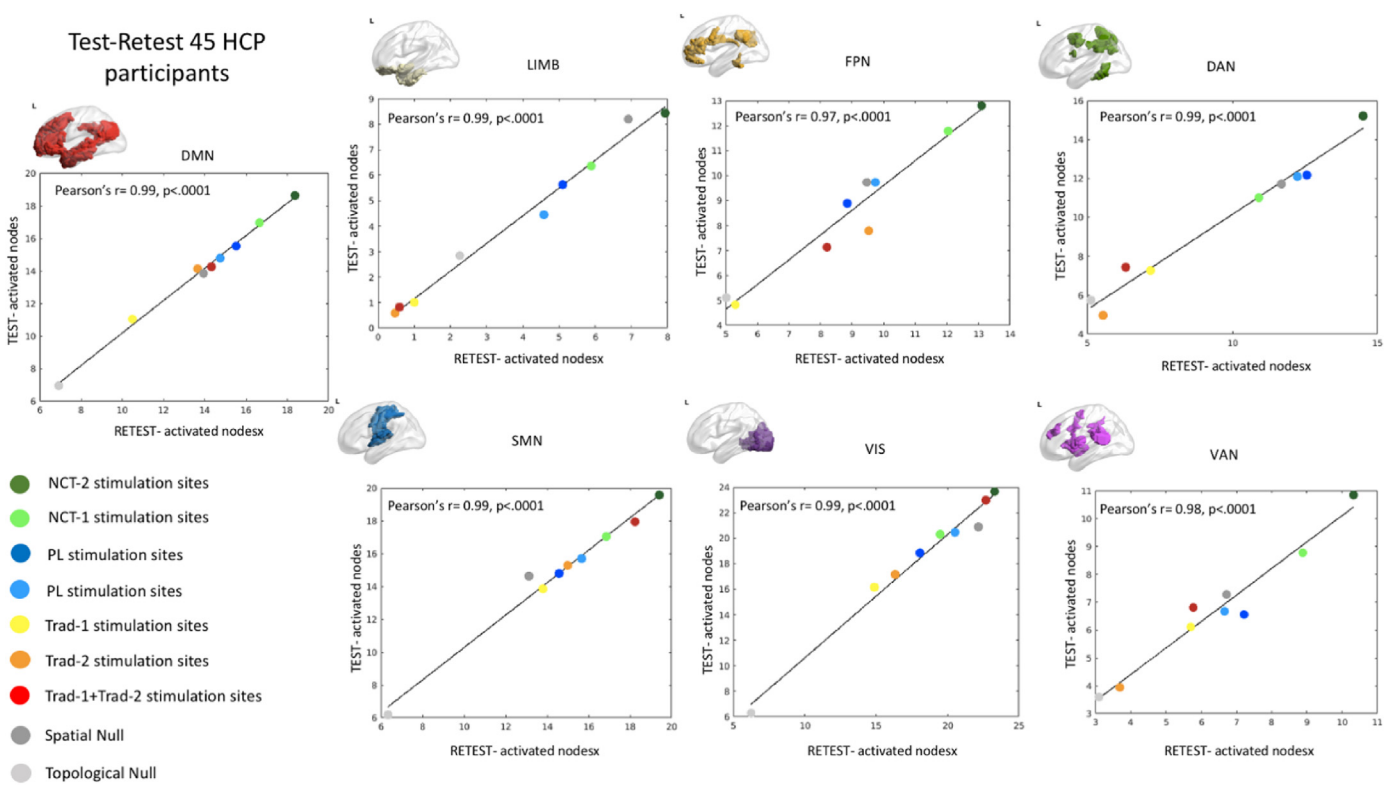

Fig. 9. Test-retest reliability. High test-retest reliability was observed for all TMS simulations. The mean number of activated nodes per condition is shown, both at test and retest, for 45 individuals. Across visits, the average amount of activated nodes by each simulation was found highly consistent, with an always greater number of activated nodes by the NCT-2 stimulation condition.

physical impediments of managing two machines simultaneously limit their practicality [78]. Nevertheless, current approaches are under development to overcome those limitations, making multi-site stimulation a foreseeable option in the future [78].

It is worth noticing that the stimulation of multiple nodes based on NCT predictions also outperformed stimulation of sites chosen based on topological properties (path length and nodal degree). As for the comparison between spatial and topological null models, we observed that the former achieves higher network activation than the latter, suggesting that the relationship between weight and distance of the brain nodes is more important than degree, weight and strength distribution in guiding propagation trajectories [61,62]. Furthermore, we observed that the personalization of stimulation sites appears to be more relevant in cognitive or high-order functional networks, than on sensory networks (i.e., VIS and SMN), where the average network engagement was relatively similar between the traditional approach and the NCT simulations. This finding appears in line with the notion that greater interindividual variability is observed in high order, task-positive networks [79]— to the point that individual brain fingerprinting has been suggested [8]— and thus they might be the networks which would benefit the most from individualized targeting.

Our last conclusion is based on the evidence that substantial differences exist in the level of engagement specificity across networks following stimulation. Indeed, high levels of precision can be observed for most networks tested, but less following stimulation of the SMN, DAN, and VAN, which tend to co-activate to some extent (Fig. 5). In the present study, we indeed observed a strong correlation between such networks in the number of white matter bundles connecting them. Of interest, those networks have also been observed to increase in their functional connectivity, from childhood to late adulthood, as a function of the topological properties of their nodes [80]. This combined evidence suggests that their strong structural and function internetwork connectivity might underlie their tendency to co-activate, as they share many pathways between their nodes. Indeed, the DAN, VAN and SMN networks share important functional roles, especially in the top-down and bottom-up control of attention and the re-orienting toward relevant stimuli for the DAN and VAN networks, respectively [81], and in the VAN control over SMN for the inhibition of behavioral responses [82].

Finally, NCT predictions for the identification of stimulation sites in the brain were not only tested on functional network engagement, but also as an approach to test the feasibility of reaching widespread regions commonly reported across clinical and research studies. We took as an example regions reported in studies on depression and cognitive control, which are at the center of many current TMS clinical and experimental trials [59,60]. In the past year alone, several studies have looked at the possibility to personalize stimulation sites in depression [83–85], based on the rationale that current applications, although effective, are limited by the fact that the optimal stimulation target remains unknown [83]. As a result, current efforts have tried to personalize stimulation either based on individualized parcels from neuroimaging data [84], or based on the mapping of symptoms' clusters [85].

In the present study, we offer an alternative to such approaches, which entirely relies on simulations run on topological models. The first advantage is that our NCT model can combine both functional and structural information, which embeds the two most crucial sources of information in stimulation paradigms: the initial state of activity of the brain prior to the stimulation delivery, and the individual fibers' map through which the signal will propagate. Secondly, since the NCT approach is based on simulations, it is possible to a priori test all possible targets in the brain to observe the induced effect on propagation and subsequently opt for the most desirable one(s). We want to stress that NCT models were indeed optimized to achieve the highest network engagement and therefore should not come surprising that they achieve high results in this direction. However, our hypothesis was that if the optimal stimulation sites are already employed in everyday TMS procedures, then we should not observe any difference between the sites predicted by the NCT model and those used routinely. One could also argue that the superior predicting performance of NCT is imputable to the fact that it comprises information captured by nodal degree. However, we controlled for this possibility by comparing stimulation based on NCT predictions to that of stimulating graph-based models (PL or ND). Furthermore, we control that the observed effects are not related to topographical properties or spatial proximity of the nodes by means of topological and spatial null models. Respectively, random graphs as built that preserve weight, degree, and strength distribution (Topological Null Model); or preserving the relationship of weight and distance between nodes (Spatial Null Model). By testing them against the predictions of NCT-derived stimulation sites we can rule out the possibility that the observed effects are solely based on those factors. Since these conditions were met, the present study highlights the possibility to improve both the efficiency and the reliability of targeting by means of predictive models based on the individual brain topology. Future studies should test NCT predictions via real TMS stimulations, comparing the effects of prior targeting choices with the one suggested by the model. Finally, even though our the NCT model was run without boundaries by testing all possible stimulation entries at the whole brain level, for most of the participants the predicted best stimulation site appeared to fall within the target network. As an example, targeting of the DMN resulted in 90% of the optimal stimulation nodes to fall within the target state. For other networks, like the FPN, SMN or DAN, percentages shifted around the 82%, 83% and 70% respectively. This result highlights the high modularity of the brain network by suggesting that it is easier to access a module by means of intra-network connections rather than inter-networks pathways. Such evidence might guide future studies in employing TMS to corroborate and further personalize network parcellations at the single subject level, a desirable step in the future of personalized medicine approaches [86].

The present study is not free of limitations. Indeed, we implemented a model based on linear dynamics, which is not representative of real brain dynamics. Nevertheless, studies continue to highlight the relevance of results in the human brain derived from the assumption of linearity [54]. Second, we did not impose cortical restrictions for the model, meaning that sometimes NCT simulations predict subcortical structures as the optimal stimulation nodes, which might not be easily reached via standard TMS. Indeed, sites are selected individually based on modeled stimulation scenarios, resulting in few subjects (out of the 400 tested) that have their optimal stimulation site located in regions of the brain that would be either inconvenient or uncomfortable to reach in real life TMS. As an example, to reach target states like the FPN, SMN or DAN network, the 80–99% of subjects have ideal target nodes in accessible locations of the brain. For the DMN, an example of the location of each individual optimal stimulation site can be found in Fig. 3, panel A. The variability in the location of the stimulation site is a crucial element in our simulations, as well as a cardinal point in this study, which we wish to stress. This is because it highlights the fact that for some individuals, the optimal driver node to ensure a state transition toward a desired direction (e.g., induce activation of a brain network, like the DMN) is located in less convenient regions compared to other individuals. This could represent an early disadvantage for some participants in a study, and it might add up to other known factors discriminating responders to non-responders in TMS interventions [87]. In this sense, to be able to

provide knowledge to the investigator on such individual conditions might help him/her in developing alternative strategies aimed at maximizing the chances of such individuals of receiving the best stimulation possible. Indeed, the fact that regions of interest in neurostimulation interventions are in hard-to-reach locations of the brain is not new. The most famous example is the relatively recent discovery of the role of the subgenual cingulate cortex in modulating depressive symptoms [83]. To overcome the limit of TMS not being able to reach deep limbic regions, recent studies have leveraged on personalized connectivity maps to identify regions in the frontal cortex that are connected to such seed, as a possible alternative. The same principle could hence been applied for individuals whose optimal stimulation site, as identified by the model, falls in inconvenient or uncomfortable brain locations, although promising alternatives might come from deep TMS devices [88]. Finally, the principles behind control theory have a wide applicability in brain stimulation interventions that expand beyond the use of TMS in humans, and include deep brain stimulation by means of intracortical electrodes [22], or controlled lesion approaches in animal models [89].

On a final note, future models might achieve an even higher amount of personalization by embedding additional information, such as oscillatory dynamics from electroencephalography recording, or individual target maps based on metabolic patterns, as via positron emission tomography [90,91]. Nodes' oscillatory frequencies and the strength of their anatomical connectivity have also been investigated to explain the distinct effects of stimulation on the functional coupling of the stimulated node to the rest of the brain [92,93]. In particular, both computational models and empirical stimulation studies support the notion that it is possible to induce large-scale neural changes in functional connectivity following the stimulation of a single node, but that those occur differently as a function of the intrinsic properties of the stimulated node [92]. Of interest, it shows that peripheral nodes, which are characterized by a weaker connectivity profile with the rest of the brain and hence show higher flexibility, have the highest chance of inducing greater changes in functional connectivity compared to central brain hubs, which are instead more hardcore and thus more resilient to perturbation [92]. These differences lead them to behave differently when exposed to the same stimulation protocol [92,93]: for example, inhibitory stimulation results in an increase in the functional coupling of peripheral nodes with the rest of the brain because it acts by decreasing their high frequency oscillatory rate thus making their activity more similar to the slower dynamics of the rest of the brain. Opposite, inhibitory stimulation applied on the slow oscillatory activity typical of core hubs helps in further decreasing their activity pattern and results in their functional disconnection with the rest of the brain [92]. Considering the importance of such findings, future studies should pay extra care in the modeling and testing of brain stimulation as a function of oscillatory brain dynamics at the time of stimulation. In our study, we informed the model on the underlying activity state of the brain by means of the BOLD signal, but future studies might need to consider online EEG recordings instead, which are more ideal for such purpose. Overall, we believe the present work has highlighted the possible use of multidisciplinary efforts in promoting personalized intervention, possibly opening the road for future applications in TMS studies.

5. Conclusions

The possibility to directly interact with the brain and manipulate its activity is becoming concrete thanks to noninvasive brain stimulation approaches. In order to optimize the efficacy of stimulation scenarios, topological models might be employed for the prior individualization of input nodes with the highest chances of recruiting regions of interest based on their spatial proximity and structural connectivity. The present work hence suggests that knowledge of the individual tractogram and activity state are useful to optimize stimulation efforts and further opens the way to guided state transitioning.

Funding

HCP is the result of efforts of co-investigators from the University of Southern California, Martinos Center for Biomedical Imaging at Massachusetts General Hospital (MGH), Washington University, and the University of Minnesota. The HCP project (Principal Investigators: Bruce Rosen, Martinos Center at Massachusetts General Hospital; Arthur W. Toga, University of Southern California, Van J. Weeden, Martinos Center at Massachusetts General Hospital) is supported by the National Institute of Dental and Craniofacial Research (NIDCR), the National Institute of Mental Health (NIMH) and the National Institute of Neurological Disorders and Stroke (NINDS). AV was partially supported by funding from "Progetto giovani ricercatori: FINAGE" (GR- 2018- 12367927) from the Italian Ministry of Health". EKT is supported by the Government of Canada's New Frontiers in Research Fund (NFRF), NFRFE-2021-00420 and by the Natural Sciences and Engineering Research Council of Canada (NSERC), funding reference number RGPIN-2021-02949. ES is supported by the NIH (R01 MH117063–01, R01 AG060981-01) and the ADDF-aFTD (ADDF-aFTD GA201902–2017902). ALB was supported by NIH 1P01HL132825 and the European Union's Horizon 2020 research and innovation programme under grant agreement No 810115 - DYNASNET.

Data availability

Structural and functional data used in the study are available from the original Human Connectome Projects dataset (https://www.humanconnectome.org/). All analyses were conducted using the following freely available codes: network dynamics were modeled by means of the code used in Stiso et al., 2019 [22]; the computation of the Characteristic Path Length, Nodal Degree and the building of Topological Null models were constructed by means of the Brain Connectivity Toolbox (https://sites.google.com/site/bctnet/); SN models were constructed based on the available code from Roberts et al., 2016 [62]. For more information contact the corresponding author or visit https://gordon.mgh.harvard.edu/gc/research/precision-neuroscience-neuromodulation-program/.

CRediT authorship contribution statement

Arianna Menardi: Conceptualization, Methodology, Formal analysis, Writing – original draft. **Davide Momi:** Conceptualization, Methodology, Formal analysis, Writing – review & editing. **Antonino Vallesi:** Conceptualization, Methodology, Writing – review & editing. **Albert-László Barabási:** Conceptualization, Methodology, Writing – review & editing. **Emma K. Towlson:** Conceptualization, Methodology, Formal analysis, Writing – review & editing, Supervision. **Emiliano Santarnecchi:** Conceptualization, Methodology, Writing – review & editing, Supervision.

Declaration of competing interest

ALB is founder of Scipher Medicine and Foodome, companies that explore the use of network-based tools in health.

Appendix A. Supplementary data

Supplementary data to this article can be found online at https://doi.org/10.1016/j.brs.2022.09.011.

References

[1] van den Heuvel MP, Sporns O. Rich-club organization of the human connectome. J Neurosci 2011;31:15775–86. https://doi.org/10.1523/JNEUROSCI.3539-11.2011.

[2] Meunier D, Lambiotte R, Bullmore ET. Modular and hierarchically modular organization of brain networks. Front Neurosci 2010;4. https://doi.org/10.3389/fnins.2010.00200.

[3] Sporns O, Kötter R. Motifs in brain networks. PLoS Biol 2004;2:e369. https://doi.org/10.1371/journal.pbio.0020369.

[4] Bassett DS, Bullmore E. Small-world brain networks. Neuroscientist 2006;12:512–23. https://doi.org/10.1177/1073858406293182.

[5] Deco G, Kringelbach ML. Hierarchy of information processing in the brain: a novel 'intrinsic ignition' framework. Neuron 2017;94:961–8. https://doi.org/10.1016/j.neuron.2017.03.028.

[6] Wang J, Zuo X, He Y. Graph-based network analysis of resting-state functional MRI. Front Syst Neurosci 2010;4. https://doi.org/10.3389/fnsys.2010.00016.

[7] Langer N, Pedroni A, Gianotti LRR, Hänggi J, Knoch D, Jäncke L. Functional brain network efficiency predicts intelligence. Hum Brain Mapp 2012;33:1393. https://doi.org/10.1002/hbm.21297.

[8] Finn ES, Shen X, Scheinost D, Rosenberg MD, Huang J, Chun MM, et al. Functional connectome fingerprinting: identifying individuals using patterns of brain connectivity. Nat Neurosci 2015;18:1664–71. https://doi.org/10.1038/nn.4135.

[9] Mueller S, Wang D, Fox MD, Yeo BTT, Sepulcre J, Sabuncu MR, et al. Individual variability in functional connectivity architecture of the human brain. Neuron 2013;77:586–95. https://doi.org/10.1016/j.neuron.2012.12.028.

[10] Lefaucheur JP, Aleman A, Baeken C, Benninger DH, Brunelin J, Di Lazzaro V, et al. Evidence-based guidelines on the therapeutic use of repetitive transcranial magnetic stimulation (rTMS): an update (2014–2018). Clin Neurophysiol 2020;131:474–528. https://doi.org/10.1016/j.clinph.2019.11.002.

[11] Valero-Cabrè A, Amengual JL, Stengel C, Pascual-Leone A, Coubard OA. Transcranial magnetic stimulation in basic and clinical neuroscience: a comprehensive review of fundamental principles and novel insights. Neurosci Biobehav Rev 2017;83:381–404. https://doi.org/10.1016/j.neubiorev.2017.10.006.

[12] Hallett M. Transcranial magnetic stimulation and the human brain. Nature 2000;406:147–50. https://doi.org/10.1038/35018000.

[13] Connolly KR, Helmer A, Cristancho MA, Cristancho P, O'Reardon JP. Effectiveness of transcranial magnetic stimulation in clinical practice post-FDA approval in the United States: results observed with the first 100 consecutive cases of depression at an academic medical center. J Clin Psychiatr 2012;73:567–73. https://doi.org/10.4088/JCP.11m07413.

[14] Schwedt TJ, Vargas B. Neurostimulation for treatment of migraine and cluster headache. Pain Med 2015;16:1827–34. https://doi.org/10.1111/pme.12792.

[15] Stultz DJ, Osburn S, Burns T, Pawlowska-Wajswol S, Walton R. Transcranial magnetic stimulation (TMS) safety with respect to seizures: a literature review. Neuropsychiatric Dis Treat 2020;16:2989. https://doi.org/10.2147/NDT.S276635.

[16] Belardinelli P, Biabani M, Blumberger DM, Bortoletto M, Casarotto S, David O, et al. Reproducibility in TMS–EEG studies: a call for data sharing, standard procedures and effective experimental control. Brain Stimul: Basic Trans Clinic Res Neuromod 2019;12:787–90. https://doi.org/10.1016/j.brs.2019.01.010.

[17] Toschi N, Welt T, Guerrisi M, Keck ME. Transcranial magnetic stimulation in heterogeneous brain tissue: clinical impact on focality, reproducibility and true sham stimulation. J Psychiatr Res 2009;43:255–64. https://doi.org/10.1016/j.jpsychires.2008.04.008.

[18] Ozdemir RA, Tadayon E, Boucher P, Momi D, Karakhanyan KA, Fox MD, et al. Individualized perturbation of the human connectome reveals reproducible biomarkers of network dynamics relevant to cognition. Proc Natl Acad Sci USA 2020:201911240. https://doi.org/10.1073/pnas.1911240117.

[19] Santolini M, Barabasi A-L. Predicting perturbation patterns from the topology of biological networks. 2018, 201720589. https://doi.org/10.1101/349324.

[20] Betzel RF, Gu S, Medaglia JD, Pasqualetti F, Bassett DS. Optimally controlling the human connectome: the role of network topology. Sci Rep 2016;6:30770. https://doi.org/10.1038/srep30770.

[21] Gu S, Pasqualetti F, Cieslak M, Telesford QK, Yu AB, Kahn AE, et al. Controllability of structural brain networks. Nat Commun 2015;6. https://doi.org/10.1038/ncomms9414.

[22] Stiso J, Khambhati AN, Menara T, Kahn AE, Stein JM, Das SR, et al. White matter network architecture guides direct electrical stimulation through optimal state transitions | elsevier enhanced reader. Cell Rep 2019;28:2554–66. https://doi.org/10.1016/j.celrep.2019.08.008.

[23] Tu C, Rocha RP, Corbetta M, Zampieri S, Zorzi M, Suweis S. Warnings and caveats in brain controllability. Neuroimage 2018;176:83–91. https://doi.org/10.1016/j.neuroimage.2018.04.010.

[24] Medaglia JD, Zurn P, Sinnott-Armstrong W, Bassett DS. Mind control as a guide for the mind. Nat Human Behav 2017;1:1–8. https://doi.org/10.1038/s41562-017-0119.

[25] Liu Y-Y, Slotine J-J, Barabási A-L. Controllability of complex networks. Nature 2011;473:167–73. https://doi.org/10.1038/nature10011.

[26] Medaglia JD, Harvey DY, White N, Kelkar A, Zimmerman J, Bassett DS, et al. Network controllability in the inferior frontal gyrus relates to controlled language variability and susceptibility to TMS. J Neurosci 2018;38:6399–410. https://doi.org/10.1523/JNEUROSCI.0092-17.2018.

[27] Van Essen DC, Smith SM, Barch DM, Behrens TEJ, Yacoub E, Ugurbil K, et al. The Wu-minn human connectome project: an overview. Neuroimage 2013;80:62–79. https://doi.org/10.1016/j.neuroimage.2013.05.041.

[28] Glasser MF, Sotiropoulos SN, Wilson JA, Coalson TS, Fischl B, Andersson JL, et al. The minimal preprocessing pipelines for the human connectome project. Neuroimage 2013;80:105. https://doi.org/10.1016/j.neuroimage.2013.04.127.

[29] Smith SM, Andersson J, Auerbach EJ, Beckmann CF, Bijsterbosch J, Douaud G, et al. Resting-state fMRI in the human connectome project. Neuroimage 2013;80:144. https://doi.org/10.1016/j.neuroimage.2013.05.039.

[30] Sotiropoulos SN, Jbabdi S, Xu J, Andersson JL, Moeller S, Auerbach EJ, et al. Advances in diffusion MRI acquisition and processing in the human connectome project. Neuroimage 2013;80:125–43. https://doi.org/10.1016/j.neuroimage.2013.05.057.

[31] Ugurbil K, Xu J, Auerbach EJ, Moeller S, Vu A, Duarte-Carvajalino JM, et al. Pushing spatial and temporal resolution for functional and diffusion MRI in the Human Connectome Project. Neuroimage 2013;80:80–104. https://doi.org/10.1016/j.neuroimage.2013.05.012.

[32] Jenkinson M, Beckmann CF, Behrens TEJ, Woolrich MW, Smith SM. FSL Neuroimage 2012;62:782–90. https://doi.org/10.1016/j.neuroimage.2011.09.015.

[33] Tournier J-D, Calamante F, Connelly A. MRtrix: diffusion tractography in crossing fiber regions. Int J Imag Syst Technol 2012;22:53–66. https://doi.org/10.1002/ima.22005.

[34] Fischl B, van der Kouwe A, Destrieux C, Halgren E, Ségonne F, Salat DH, et al. Automatically parcellating the human cerebral cortex. Cerebr Cortex 2004;14:11–22. https://doi.org/10.1093/cercor/bhg087.

[35] Andersson JLR, Sotiropoulos SN. An integrated approach to correction for off-resonance effects and subject movement in diffusion MR imaging. Neuroimage 2016;125:1063–78. https://doi.org/10.1016/j.neuroimage.2015.10.019.

[36] Glasser MF, Smith SM, Marcus DS, Andersson JLR, Auerbach EJ, Behrens TEJ, et al. The Human Connectome Project's neuroimaging approach. Nat Neurosci 2016;19:1175–87. https://doi.org/10.1038/nn.4361.

[37] Christiaens D, Reisert M, Dhollander T, Sunaert S, Suetens P, Maes F. Global tractography of multi-shell diffusion-weighted imaging data using a multi-tissue model. Neuroimage 2015;123:89–101. https://doi.org/10.1016/j.neuroimage.2015.08.008.

[38] Jeurissen B, Tournier J-D, Dhollander T, Connelly A, Sijbers J. Multi-tissue constrained spherical deconvolution for improved analysis of multi-shell diffusion MRI data. Neuroimage 2014;103:411–26. https://doi.org/10.1016/j.neuroimage.2014.07.061.

[39] Zhang Y, Brady M, Smith S. Segmentation of brain MR images through a hidden Markov random field model and the expectation-maximization algorithm. IEEE Trans Med Imag 2001;20:45–57. https://doi.org/10.1109/42.906424.

[40] Amico E, Bodart O, Rosanova M, Gosseries O, Heine L, Van Mierlo P, et al. Tracking dynamic interactions between structural and functional connectivity: a TMS/EEG-dMRI study. Brain Connect 2017;7:84–97. https://doi.org/10.1089/brain.2016.0462.

[41] Tournier J-D, Calamante F, Connelly A. Improved probabilistic streamlines tractography by 2nd order integration over fibre orientation distributions. 2010. p. 1.

[42] Smith RE, Tournier J-D, Calamante F, Connelly A. SIFT2: enabling dense quantitative assessment of brain white matter connectivity using streamlines tractography. Neuroimage 2015;119:338–51. https://doi.org/10.1016/j.neuroimage.2015.06.092.

[43] Schaefer A, Kong R, Gordon EM, Laumann TO, Zuo X-N, Holmes AJ, et al. Local-global parcellation of the human cerebral cortex from intrinsic functional connectivity MRI. Cerebr Cortex 2018;28:3095–114. https://doi.org/10.1093/cercor/bhx179.

[44] Fischl B, Sereno MI, Tootell RB, Dale AM. High-resolution intersubject averaging and a coordinate system for the cortical surface. Hum Brain Mapp 1999;8:272–84. https://doi.org/10.1002/(sici)1097-0193(1999)8:4<272::aid-hbm10>3.0.co;2-4.

[45] Buckner RL, Krienen FM, Castellanos A, Diaz JC, Yeo BTT. The organization of the human cerebellum estimated by intrinsic functional connectivity. J Neurophysiol 2011;106:2322. https://doi.org/10.1152/jn.00339.2011.

[46] Bonilha L, Gleichgerrcht E, Fridriksson J, Rorden C, Breedlove JL, Nesland T, et al. Reproducibility of the structural brain connectome derived from diffusion tensor imaging. PLoS One 2015;10. https://doi.org/10.1371/journal.pone.0135247.

[47] Rubinov M, Sporns O. Complex network measures of brain connectivity: uses and interpretations. Neuroimage 2010;52:1059–69. https://doi.org/10.1016/j.neuroimage.2009.10.003.

[48] Momi D, Neri F, Coiro G, Smeralda C, Veniero D, Sprugnoli G, et al. Cognitive enhancement via network-targeted cortico-cortical associative brain stimulation. Cerebr Cortex 2020;30:1516–27. https://doi.org/10.1093/cercor/bhz182.

[49] Kim JZ, Bassett DS. Linear dynamics and control of brain networks. Neural Engineering 2020:497–518. https://doi.org/10.1007/978-3-030-43395-6_17.
[50] Honey CJ, Sporns O, Cammoun L, Gigandet X, Thiran JP, Meuli R, et al. Predicting human resting-state functional connectivity from structural connectivity. Proc Natl Acad Sci USA 2009;106:2035–40. https://doi.org/10.1073/pnas.0811168106.
[51] Coron JM. Control and nonlinearity. Providence, Rhode Island: American Mathematical Society; 2009.
[52] Muldoon SF, Pasqualetti F, Gu S, Cieslak M, Grafton ST, Vettel JM, et al. Stimulation-based control of dynamic brain networks. PLoS Comput Biol 2016;12:e1005076. https://doi.org/10.1371/journal.pcbi.1005076.
[53] Whalen AJ, Brennan SN, Sauer TD, Schiff SJ. Observability and controllability of nonlinear networks: the role of symmetry. Phys Rev X 2015;5:011005. https://doi.org/10.1103/PhysRevX.5.011005.
[54] Nozari E, Stiso J, Caciagli L, Cornblath EJ, He X, Bertolero MA, et al. Is the brain macroscopically linear? A system identification of resting state dynamics. 2020.
[55] Tang E, Giusti C, Baum GL, Gu S, Pollock E, Kahn AE, et al. Developmental increases in white matter network controllability support a growing diversity of brain dynamics. Nat Commun 2017;8:1–16. https://doi.org/10.1038/s41467-017-01254-4.
[56] Tang E, Bassett DS. Colloquium: control of dynamics in brain networks. Rev Mod Phys 2018;90:031003. https://doi.org/10.1103/RevModPhys.90.031003.
[57] Parkes L, Moore TM, Calkins ME, Cieslak M, Roalf DR, Wolf DH, et al. Network controllability in transmodal cortex predicts positive psychosis spectrum symptoms. Biol Psychiatr 2021;90:409–18. https://doi.org/10.1016/j.biopsych.2021.03.016.
[58] Kenett YN, Beaty RE, Medaglia JD. A computational network control theory analysis of depression symptoms. Personal Neurosci 2018;1. https://doi.org/10.1017/pen.2018.15.
[59] Corlier J, Burnette E, Wilson AC, Lou JJ, Landeros A, Minzenberg MJ, et al. Effect of repetitive transcranial magnetic stimulation (rTMS) treatment of major depressive disorder (MDD) on cognitive control. J Affect Disord 2020;265:272–7. https://doi.org/10.1016/j.jad.2020.01.068.
[60] Modirrousta M, Meek BP, Sareen J, Enns MW. Impaired trial-by-trial adjustment of cognitive control in obsessive compulsive disorder improves after deep repetitive transcranial magnetic stimulation. BMC Neurosci 2015;16:1–9. https://doi.org/10.1186/s12868-015-0205-z.
[61] Bassett DS, Greenfield DL, Meyer-Lindenberg A, Weinberger DR, Moore SW, Bullmore ET. Efficient physical embedding of topologically complex information processing networks in brains and computer circuits. PLoS Comput Biol 2010;6:e1000748. https://doi.org/10.1371/journal.pcbi.1000748.
[62] Roberts JA, Perry A, Lord AR, Roberts G, Mitchell PB, Smith RE, et al. The contribution of geometry to the human connectome. Neuroimage 2016;124:379–93. https://doi.org/10.1016/j.neuroimage.2015.09.009.
[63] Koch G, Bonnì S, Pellicciari MC, Casula EP, Mancini M, Esposito R, et al. Transcranial magnetic stimulation of the precuneus enhances memory and neural activity in prodromal Alzheimer's disease. Neuroimage 2018;169:302–11. https://doi.org/10.1016/j.neuroimage.2017.12.048.
[64] Pievani M, Pini L, Ferrari C, Pizzini FB, Boscolo Galazzo I, Cobelli C, et al. Coordinate-based meta-analysis of the Default Mode and salience network for target identification in non-invasive brain stimulation of alzheimer's disease and behavioral variant frontotemporal dementia networks. J Alzheim Dis 2017;57:825–43. https://doi.org/10.3233/JAD-161105.
[65] Kalbe E, Schlegel M, Sack AT, Nowak DA, Dafotakis M, Bangard C, et al. Dissociating cognitive from affective theory of mind: a TMS study. Cortex 2010;46:769–80. https://doi.org/10.1016/j.cortex.2009.07.010.
[66] Tik M, Hoffman A, Sladky R, Tomova L, Hummer A, Navarro de Lara L, et al. Towards understanding rTMS mechanism of action: stimulation of the DLPFC causes network-specific increase in functional connectivity. Neuroimage 2017;162:289–96. https://doi.org/10.1016/j.neuroimage.2017.09.022.
[67] MacDonald PA, Paus T. The role of parietal cortex in awareness of self-generated movements: a transcranial magnetic stimulation study. Cerebr Cortex 2003;13:962–7. https://doi.org/10.1093/cercor/13.9.962.
[68] Postle BR, Ferrarelli F, Hamidi M, Feredoes E, Massimini M, Peterson M, et al. Repetitive transcranial magnetic stimulation dissociates working memory manipulation from retention functions in the prefrontal, but not posterior parietal, cortex. J Cognit Neurosci 2006;18:1712–22. https://doi.org/10.1162/jocn.2006.18.10.1712.
[69] Anderkova L, Pizem D, Klobusiakova P, Gajdos M, Koritakova E, Rektorova I. Theta burst stimulation enhances connectivity of the dorsal attention network in young healthy subjects: an exploratory study. Neural Plast 2018;2018. https://doi.org/10.1155/2018/3106918.
[70] Paus T, Sipila PK, Strafella AP. Synchronization of neuronal activity in the human primary motor cortex by transcranial magnetic stimulation: an EEG study. J Neurophysiol 2001;86:1983–90. https://doi.org/10.1152/jn.2001.86.4.1983.
[71] Corthout E, Uttl B, Walsh V, Hallett M, Cowey A. Timing of activity in early visual cortex as revealed by transcranial magnetic stimulation. Neuroreport 1999;10:2631–4.
[72] Lega C, Santandrea E, Ferrante O, Serpe R, Dolci C, Baldini E, et al. Modulating the influence of recent trial history on attentional capture via transcranial magnetic stimulation (TMS) of right TPJ. Cortex 2020;133:149–60. https://doi.org/10.1016/j.cortex.2020.09.009.
[73] Kavanaugh BC, Aaronson ST, Clarke GN, Holtzheimer PE, Johnson CW, McDonald WM, et al. Neurocognitive effects of repetitive transcranial magnetic stimulation with a 2-coil device in treatment-resistant major depressive disorder. J ECT 2018;34:258–65. https://doi.org/10.1097/YCT.0000000000000494.
[74] Yeh F-C, Panesar S, Fernandes D, Meola A, Yoshino M, Fernandez-Miranda JC, et al. Population-averaged atlas of the macroscale human structural connectome and its network topology. Neuroimage 2018;178:57–68. https://doi.org/10.1016/j.neuroimage.2018.05.027.
[75] Rossini PM, Barker AT, Berardelli A, Caramia MD, Caruso G, Cracco RQ, et al. Non-invasive electrical and magnetic stimulation of the brain, spinal cord and roots: basic principles and procedures for routine clinical application. Report of an IFCN committee. Electroencephalogr Clin Neurophysiol 1994;91:79–92. https://doi.org/10.1016/0013-4694(94)90029-9.
[76] Chiappini E, Silvanto J, Hibbard PB, Avenanti A, Romei V. Strengthening functionally specific neural pathways with transcranial brain stimulation. Curr Biol 2018;28:R735–6. https://doi.org/10.1016/j.cub.2018.05.083.
[77] Santarnecchi E, Momi D, Sprugnoli G, Neri F, Pascual-Leone A, Rossi A, et al. Modulation of network-to-network connectivity via spike-timing-dependent noninvasive brain stimulation. Hum Brain Mapp 2018. https://doi.org/10.1002/hbm.24329.
[78] Koponen LM, Nieminen JO, Ilmoniemi RJ. Multi-locus transcranial magnetic stimulation—theory and implementation. Brain Stimul 2018;11:849–55. https://doi.org/10.1016/j.brs.2018.03.014.
[79] Gordon EM, Laumann TO, Gilmore Adrian W, Newbold DJ, Greene DJ, Berg JJ, et al. Precision functional mapping of individual human brains. Neuron 2017;95:791–807. https://doi.org/10.1016/j.neuron.2017.07.011. e7.
[80] Betzel RF, Byrge L, He Y, Goni J, Zuo X-N, Sporns O. Changes in structural and functional connectivity among resting-state networks across the human lifespan. Neuroimage 2014;102:345–57. https://doi.org/10.1016/j.neuroimage.2014.07.067.
[81] Corbetta M, Patel G, Shulman GL. The reorienting system of the human brain: from environment to theory of mind. Neuron 2008;58:306–24. https://doi.org/10.1016/j.neuron.2008.04.017.
[82] Aron AR. The neural basis of inhibition in cognitive control. Neuroscientist 2007;13:214–28. https://doi.org/10.1177/1073858407299288.
[83] Cash RFH, Weigand A, Zalesky A, Siddiqi SH, Downar J, Fitzgerald PB, et al. Using brain imaging to improve spatial targeting of transcranial magnetic stimulation for depression. Biol Psychiatr 2020. https://doi.org/10.1016/j.biopsych.2020.05.033. In Press:12.
[84] Moreno-Ortega M, Kangarlu A, Lee S, Perera T, Kangarlu J, Palomo T, et al. Parcel-guided rTMS for depression. Transl Psychiatry 2020;10:1–6. https://doi.org/10.1038/s41398-020-00970-8.
[85] Nestor SM, Blumberger DM. Mapping symptom clusters to circuits: toward personalizing TMS targets to improve treatment outcomes in depression. Am J Psychiatr 2020. https://doi.org/10.1176/appi.ajp.2020.20030271.
[86] Wang D, Buckner RL, Fox MD, Holt DJ, Holmes AJ, Stoecklein S, et al. Parcellating cortical functional networks in individuals. Nat Neurosci 2015;18:1853–60. https://doi.org/10.1038/nn.4164.
[87] Shah-Basak PP, Harvey DY, Parchure S, Faseyitan O, Sacchetti DL, Ahmed A, et al. Brain-derived neurotrophic factor polymorphism influences response to single-pulse transcranial magnetic stimulation at rest. Neuromodulation: Technol Neural Interface 2021;24:854–62. https://doi.org/10.1111/ner.13287.
[88] Gomez-Tames J, Hamasaka A, Hirata A, Laakso I, Lu M, Ueno S. Group-level analysis of induced electric field in deep brain regions by different TMS coils. Phys Med Biol 2020;65:025007. https://doi.org/10.1088/1361-6560/ab5e4a.
[89] Yan G, Vértes PE, Towlson EK, Chew YL, Walker DS, Schafer WR, et al. Network control principles predict neuron function in the Caenorhabditis elegans connectome. Nature 2017;550:519–23. https://doi.org/10.1038/nature24056.
[90] Esposito R, Bortoletto M, Miniussi C. Integrating TMS, EEG, and MRI as an approach for studying brain connectivity. Neuroscientist 2020;26:471–86. https://doi.org/10.1177/1073858420916452.
[91] Arabkheradmand G, Krieg TD, Salinas FS, Fox PT, Mogul DJ. Predicting TMS-induced activation in human neocortex using concurrent TMS/PET, finite element analysis and computational modeling. Biomed Phys Eng Express 2019;5:025028. https://doi.org/10.1088/2057-1976/aaf202.
[92] Gollo LL, Roberts JA, Cocchi L. Mapping how local perturbations influence systems-level brain dynamics. Neuroimage 2017;160:97–112. https://doi.org/10.1016/j.neuroimage.2017.01.057.
[93] Cocchi L, Sale MV, Gollo LL, Bell PT, Nguyen VT, Zalesky A, et al. A hierarchy of timescales explains distinct effects of local inhibition of primary visual cortex and frontal eye fields. Elife 2016;5. https://doi.org/10.7554/eLife.15252.